Reducing Noise and Vibration of Hydraulic Hybrid And Plug-In Hybrid Electric Vehicles

Final Report

By

Mohammad Elahinia
Associate Professor
Department of Mechanical, Industrial and Mechanical Engineering
College of Engineering

Prepared for The University of Toledo University Transportation Center and the U.S. Department of Transportation

February 2012

DISCLAIMER

The contents of this report reflect the views of the authors, who are responsible for the facts and the accuracy of the information presented herein. This document is disseminated under the sponsorship of the Department of Transportation University Transportation Centers Program, in the interest of information exchange. The U.S. Government assumes no liability for the contents or use thereof.

Abstract

The University of Toledo University Transportation Center (UT-UTC) has identified hybrid vehicles as one of the three areas of the research. The activities in this research are directed towards the noise, vibration, and harshness (NVH) solutions for hybrid vehicles. The soaring fuel prices require imperious steps in developing alternate propulsion technologies. The design and development of hybrid vehicles is a critical issue for an economy dependent on an efficient, fast, and secure transportation system. To date, better fuel economy has been mainly achieved by combining two propulsion sources (hybridization) and/or by developing better managing algorithms for the internal combustion engines. Examples for the hybridization are the plug-in hybrid electric and the hydraulic-hybrid vehicles. An example of managing internal combustion engines is the cylinder on demand as a solution that Honda has recently introduced. One common problem with these solutions is excessive noise and vibration that is caused by switching between the propulsion sources and propulsion modes. To mitigate this problem there is a need to develop vibration isolation devices that can provide isolation over a wide range of frequencies. This research sought to study the NVH problem of the hybrid vehicles and to introduce isolation mounts to overcome these issues.

Hydraulic and elastomeric mounts are generally used to dynamically isolate engines and power trains from the chassis, while statically holding these elements together. Hydraulic mounts overcome some of the drawbacks of the elastomeric mounts. The stiffness and damping of the hydraulic mounts varies with frequency and amplitude of vibration. It is possible to design a hydraulic mount that has a significantly larger static stiffness, compared to an elastomeric mount, and has a much smaller dynamic stiffness at a specific frequency. To achieve low vibration transmissibility, the mount can be tuned to the primary frequency of the vibration source. On the other hand, to isolate the high frequency vibration of the engine, the mount should have low stiffness and low damping, which is not possible to achieve.

This project consisted of four phases with the overall goal of developing a semi-active mount, which was successfully realized. It was shown that the semi-active mount improved the existing hydraulic mounts. This semi-active mount was developed through adding a magnetorheological (MR) fluid element. In response to magnetic fields, MR fluids change their viscosity, which can be harnessed in a variable stiffness and damping mount. The resulting mount provides shock and vibration isolation over a wide range of frequencies. This extended isolation frequency range is achieved through the variable dynamic stiffness of the MR portion of the mount. This solution makes it possible to improve the noise and vibration characteristic of hybrid vehicles with alternative propulsion systems.

Technical Approach or Methodology

It was proposed to develop an MR fluid based semi-active mount by modifying the existing hydraulic mounts. In this design, the existing mount was modified to adapt the MR fluid technology in the hydraulic part of the mount. Specifically, the hydraulic fluid was substituted with MR fluid and two coils were added to provide the magnetic field required to excite the fluid. The research activities for the four phases of the grant are the following.

Stage 1:

Perform sensitivity analysis
Design the mount based on sensitivity analysis
Developing a mathematical model for the MR mount

Stage 2:

Implementing the MR fluid behavior model
Simulate the semi-active mount
Correlating with hydraulic mount data

Stage 3:

Design a control algorithm based on the mathematical model and simulation results

Stage 4:

Implement the control algorithm experimentally and evaluate the performance of the mount in closed-loop.

As highlighted in this report, as well as the publications which resulted from this work, these goals were successfully achieved. Additionally, several graduate students were trained on various technical and scientific aspects of this project. Two Ph.D. students and two masters students completed their graduate studies while working on the four phases of this project.

Publications

The following is the list of publications, which resulted by the end of the last three phases of the project:

Journal papers:

1. Nguyen, T. M. and Elahinia, M. H., “Vibration Isolation for Hydraulic Hybrid Vehicles,” Journal of Shock and Vibration, February 2008, 15(2):193-204.
2. Nguyen, T. M., Ciocanel, C., and Elahinia, M. H., “A squeeze-flow mode magnetorheological mount: design, modeling, and experimental evaluation,” Journal of Vibration & Acoustics – Transactions of the ASME, April 2012, 134(2):021013-1-11.
3. Wang, S., Elahinia, M., and Nguyen, T., " Displacement and Force Control with a Mixed Mode MR Mount", Journal of Shock and Vibration, in review.
4. Nguyen, T., Wang, S., Elahinia, M., "Hydraulic Hybrid Vehicle vibration isolation control with magnetorheological fluid mounts", International Journal of

Vehicle Design, Smart Materials and Structures in Automotive Applications, in review.

Conference papers:

1. Ciocanel, C., Nguyen, T., Elahinia, M. and Naganathan, N. G., "On the Design of a Combined Squeeze-Flow Mode Magnetorheological Fluid Mount," SPIE Smart Structures and Materials, March 14-22, 2007, San Diego, California.
2. Mohaghegh Motlagh, A., Elahinia, M. H., Abuhaiba, M., and Olson, W., "Application of Smart Materials for Noise and Vibration of Hydraulic Systems," ASME DETC/CIE, September 4-7, 2007, Las Vegas, Nevada.
3. Nguyen, T., Ciocanel, C. Schroeder, C. and Elahinia M., "On the Design and Control of a Squeeze-Flow Mode Magnetorheological Fluid Mount," ASME DETC/CIE, September 4-7, 2007, Las Vegas, Nevada.
4. Nguyen, T., Ciocanel, C., and Elahinia M., "Performance of an Adaptive Magnetorheological Fluid Mount," ASME International Mechanical Engineering Congress, November 11-15, 2007, Seattle, Washington.
5. Nguyen, T. M., Ciocanel, C., Schroeder, C., and Elahinia, M. H., "Performance of a Mixed Mode MR Mount," 10th Cansmart Meeting International Workshop on Smart Materials and Structures, October 10-11, 2007, Montreal, Quebec, Canada.
6. Ciocanel, C., Nguyen, T., and Elahinia, M., "Design and modeling of a mixed mode magnetorheological (MR) fluid mount," SPIE Smart Structures and Materials, March 9-13, 2008, San Diego, California.
7. Ciocanel, C., Nguyen, T., M., Schroeder, C., and Elahinia, M. H., "Performance evaluation of a semi-active magnetorheological mount," SAE 2008 World Congress, April 14-17, 2008, Detroit, Michigan
8. Ciocanel, C., Nguyen, T., M., and Elahinia, M. H., "An Adaptive Magneto-hydraulic Vibration Isolator," 3rd International Conference, Advanced Concepts in Mechanical Engineering, Iaşi, Romania, 5 - 6 June 2008.
9. Nguyen, T., Ciocanel, C. and Elahinia M., "Parameter optimization in designing an MR mount," 15th International Congress on Sound and Vibration, 6-10 July 2008, Daejeon, Korea
10. Nguyen, T., Ciocanel, C. and Elahinia, M. H., "Theoretical and experimental development of a semi-active mount," ASME International Mechanical Engineering Congress, October 31 - November 6, 2008, Boston, Massachusetts.
11. Mohaghegh Motlagh, A., and Elahinia, M. H., "Research Simulation of a Series Hydraulic Hybrid Vehicle to Study Noise and Vibration," ASME International Mechanical Engineering Congress, October 31 - November 6, 2008, Boston, Massachusetts.
12. Nguyen, T. M., Ciocanel, C. and Elahinia, M., "Analytical modeling and experimental validation of a magnetorheological mount" Proceedings of SPIE Smart Structures and Materials, March 8-12, 2009, San Diego, California.
13. Anderson, W., Elahinia, M., and Nguyen, T., "Vibration Mitigation with a Multi-axial Magnetorheological Mount," SMASIS09 ASME Conference on Smart Materials, Adaptive Structures and Intelligent Systems September 20 - September 24, 2009, Oxnard, California.

14. Nguyen, T., Ciocanel, C. and Elahinia, M. H., A Magnetorheological Mount for Hydraulic Hybrid Vehicles," SMASIS09 ASME Conference on Smart Materials, Adaptive Structures and Intelligent Systems September 20 - September 24, 2009, Oxnard, California.
15. Anderson, W. and Elahinia M., "Multidirectional vibration isolation through the use of magnetorheological fluid technology," Proceedings of the 15th Asia Pacific Automotive Engineering Conference, October 25-29, 2009, Hanoi, Vietnam.
16. Nguyen, T. Ciocanel, C. and Elahinia M., "Structural considerations in designing magnetorheological fluid mounts," Proceedings SPIE Active and Passive Smart Structures and Integrated Systems, 7 - 11 March 2010, San Diego, CA.
17. Anderson, W. Ciocanel, C. and Elahinia, M. "A Geometric Parametric Analysis of a Magnetorheological Engine Mount," ASME International Design Engineering Technical Conferences (IDETC), August 15-18 2010, Montreal.
18. Wang, S. The, N. Anderson, W. Ciocanel, C. and Elahinia, M., "Skyhook Control of a Mixed Mode Magnetorheological Fluid Mount," ASME International Design Engineering Technical Conferences (IDETC), August 15-18 2010, Montreal.
19. Anderson, W. Wang S. Nguyen, T. Ciocanel, C. Elahinia, M. "Comparison of a hydraulic engine mount to a magnetorheological engine mount," SAE Commercial Vehicle Engineering Congress, October 5-8, 2010, Rosemont, Illinois.
20. Wang, S. Elahinia, M. The, N. Anderson, W. and Ciocanel, C., "Analysis and Control of Displacement Transmissibility and Force Transmissibility for a Two DOF Model Based on Quarter Car Concept using a Mixed Mode Magnetorheological Fluid Mount," SAE Commercial Vehicle Engineering Congress, October 5-8, 2010, Rosemont, Illinois.
21. Wang, S. and Elahinia, M. "Experimental Verification of Controllability of A Mixed Mode MR Fluid Mount," SMASIS11 ASME Conference on Smart Materials, Adaptive Structures and Intelligent Systems September 19 - 21, 2011, Scottsdale, Arizona.

Detailed Technical Report

This section of the report includes the details of the technical achievements of the research. A Magnetorheological (MR) mount has been developed to replace hydraulic mounts because the MR effect makes the mount controllable and more adaptive. This mount was designed, mathematically modeled, developed and its open-loop and closed-loop performances were experimentally investigated. Control systems were designed and evaluated in both simulation and experimentation.

The novel design of the MR mount is expected to be functional in a wide range of frequencies. More specifically, a fluid mount with a higher number of inertia tracks has a higher notch frequency (lowest dynamic stiffness point). Utilizing this fact, a wide-bandwidth MR mount is designed as explained in this following section.

Design of the MR mount

A cutout view of the mount is shown in Fig. 1. The main components of the mount are numbered as follows: 1—upper rubber part, 2—bottom rubber part, 3—inner coil, 4—inner coil housing, 5—outer coil, 6—outer coil housing, 7—flow passage,8—mount housing, 9—closing ring, 10—upper mount in connecting rod, 11—upper squeeze plate, 12—lower mounting connecting rod. The middle assembly, i.e., components 3–6, separates the inner volume of the mount into two chambers: The upper chamber that is enclosed by the top rubber (1), and the lower chamber that is enclosed by the bottom rubber (2). The MR fluid, not shown in Fig. 1, flows between the upper and lower chambers via flow passages (7) located within the middle assembly. The housing is comprised of part (8) and the closing collar (9). The mount is assembled by tightening the collar against the housing with eights screws (not shown in Fig. 1). Pictures of the actual mount are included in the Appendix. The upper rubber part has to support the static load applied to the mount (i.e., the engine block), while the bottom rubber is necessary to contain the MR fluid. Accordingly, the upper rubber has very low compliance while the bottom rubber has very high compliance. However, the upper rubber part is configured such that, despite its low compliance, it bulges when the fluid does not flow through the flow channel and/or the mount squeeze mode plates are not touching. The inner coil (3) provides the magnetic field that activates the squeeze mode, while the outer coil (5) generates the field that activates the flow mode. The inner and outer coils are enclosed in housing, (4) and (6), made of 1018 high magnetic permeability steel.

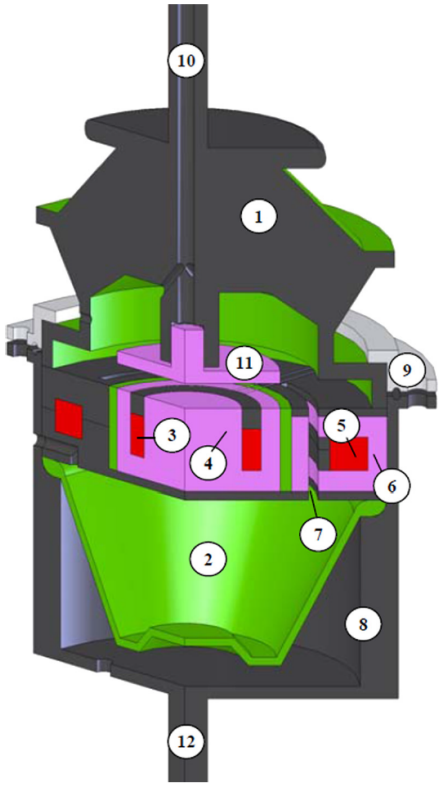

Figure 1 Section view of the MR mount

The top rubber is molded around screw (10) that serves two purposes in this design—to attach the mount to the supported mass (the engine) and to support the plate (11). The bottom surface of the plate (11) and the top surface of the housing (4) are the surfaces between which squeezing of the MR fluid happens during mount operation. The parts shown in gray and silver colors in Fig.1 are made of nonmagnetic materials.

Magnetic circuit design: This section describes the components of the magnetic circuit. The configuration of the middle assembly, consisting of elements (3)–(7), plays a major role in creating the desired characteristics of the mount. Figure 2 shows the inner coil subassembly, which activates the fluid in the squeeze mode. This subassembly consists of a magnetic yoke and core (4) that houses the circumferential coil (3). A nonmagnetic aluminum ring (shown in black in Figure 2) is used to secure the coil inside the yoke. The squeeze plate (11) is parallel to the inner coil subassembly's top surface. This plate guides the magnetic flux to be perpendicular to the two squeezing surfaces as shown in Fig. 2(b). When magnetic flux is present, the particles in the MR fluid between the two surfaces will align with the field and form chains in the vertical direction. This will increase the fluid's load carrying capacity in the direction of the external motion.

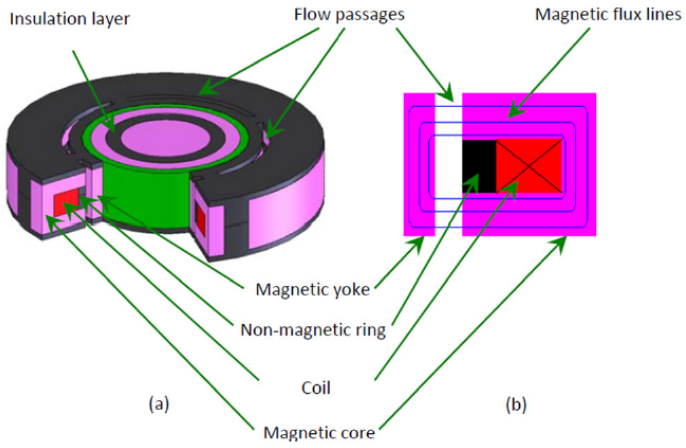

Figure 2 Outer coil subassembly for flow mode (inner coil assembly is also shown in the center): (a) Isometric section view and (b) front section view

The outer coil subassembly, as shown in Fig. 3, provides the magnetic field that activates the fluid in flow mode. As Fig. 3(a)shows, the outer coil subassembly is located outside of the inner coil subassembly. An isolation layer made of acrylic separates these two subassemblies. There are four flow passages arranged in an annular shape. The separation between the two adjacent passages is small enough to be negligible. Therefore, in the analysis, the four passages are assumed to behave similarly to a complete annular conduit. The outer coil is housed in the magnetic core that conducts the magnetic flux toward the magnetic yoke located on the other side of the flow channels. As a result,

the magnetic flux lines close through the flow passages and activate the MR fluid such that the particles inside the fluid will form chains in the horizontal direction obstructing the flow between the two chambers.

Activation of the fluid inside the flow channels and between the plates can be done simultaneously or separately in correlation with the magnitude of the input excitation. If only the outer coil is activated, the mount operates in flow mode, while if only the inner coil is activated, the mount works in squeeze mode. In the current design, the gap of the flow passages is 2.5 mm and the gap between the squeeze plates is 2 mm (after the static load is applied). The thickness and length of the flow passages, together with the squeeze mode gap, were chosen to achieve the maximum magnetic field strength within the passage and between the plates with relatively small coils. The analysis that supported this decision is described in the following section.

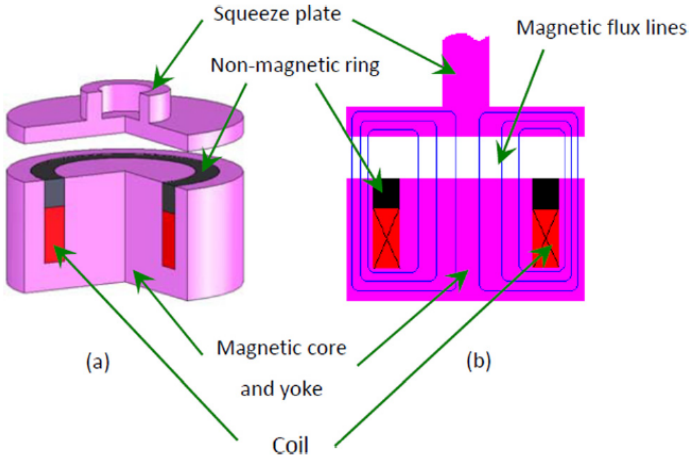

Figure 3 Inner coil subassembly for squeeze mode: (a) Isometric section view and (b) front section view

Magnetic filed analysis: One of the key elements to an efficient MR fluid based mount is the magnetic field circuit design. An ideal magnetic circuit for an MR mount should generate a magnetic field large enough to activate the fluid in the desired yield stress range without requiring a high electric current. Keeping the electric current at a low level (e.g., below 2.5 A) minimizes the heat generated during fluid activation and minimizes the required electric power. Also, the magnitude and uniformity of the magnetic field inside the flow channels and between the squeeze plates affect the mount response.

To establish the optimal geometry of the middle assembly components, simulations were performed using Maxwell 2D and 3D field simulators and ElectroMagneticWorks. The volume of the coils was constrained in order to keep the overall size of the mount similar to an existing hydraulic mount. Through simulation, the geometry of the flow passage and the electric current of the coils were varied until the geometry yielding the desired magnetic field distribution was found. A summary of the results of these simulations is provided in Figs. 4–6.

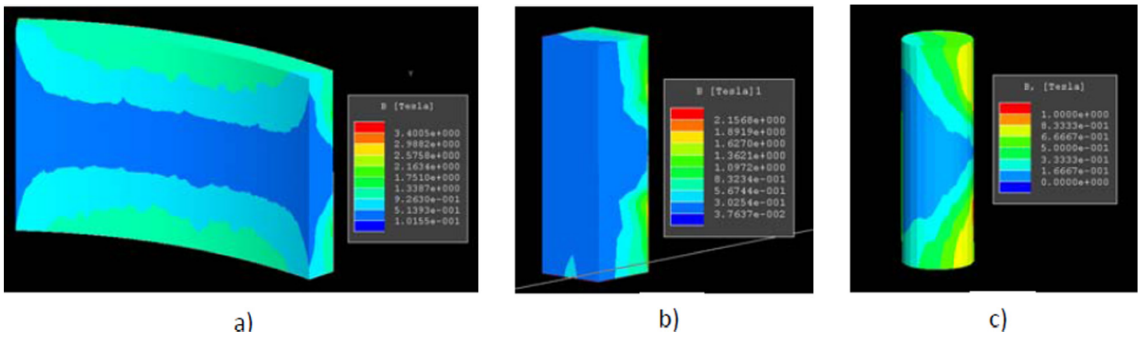

a) b) c)

Figure 4 Magnetic flux density distribution within flow conduits with different geometries for 1 A electric current feeding the coils: (a) Rectangular 2.5 mm gap, (b) square 5 mm side, and (c) circular 5 mm diameter

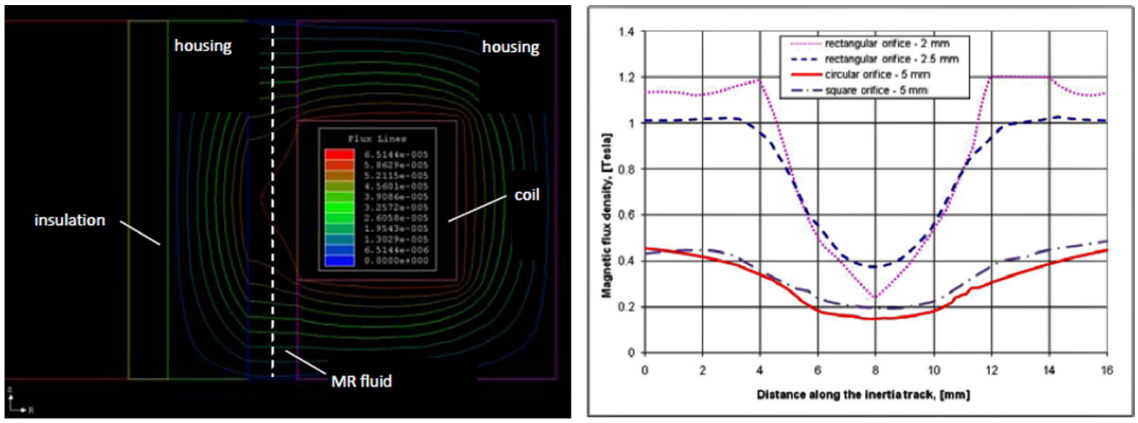

a) b)

Figure 5 (a) Magnetic flux line paths in a cross section cut through the outer magnetic circuit; (b) magnetic flux density variation along the vertical midline (the white dashed line shown in (a)) of the flow conduit with different geometries. The applied current was 1 A in all cases.

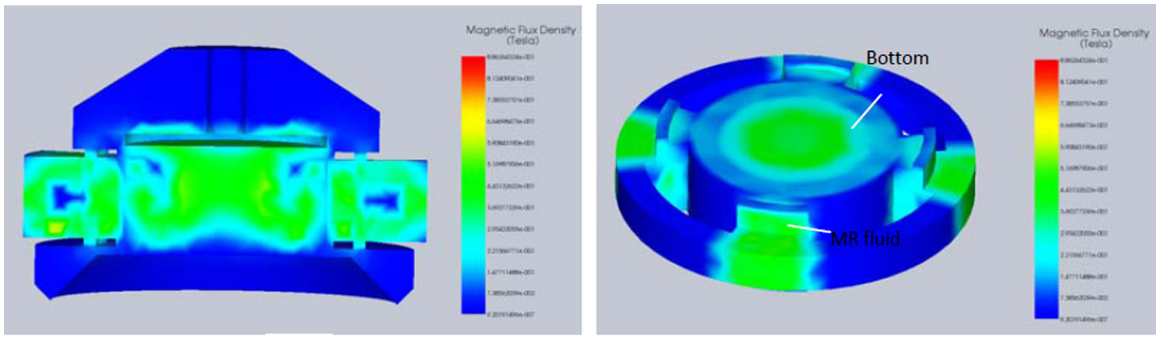

a) b)

Figure 6 (a) Cross sectional view of the mount with the coils supplied with a 1 A electric current. (b) Overall field distribution

Figure 4 shows simulated results for the magnetic flux distribution/magnetic induction in the MR fluid volume inside the flow passage. These results indicate that the rectangular duct, 2.5 mm wide, has a more uniform field distribution across it compared to square and circular tracks with similar cross section areas. In addition, in the rectangular configuration, the magnetic flux density reaches the largest values for the same value of electric current passing through the coils.

In low frequency, the narrower gap (i.e., the rectangular duct) leads to higher damping, but the opposite effect happens in high frequency. At high frequency, the oscillation is very fast and as the passage is activated, the fluid is almost restricted from entering the flow passage. As a result, the fluid volume in the upper chamber will bulge the top rubber. Thus, the small gap size may reduce the fluid's hydraulic contribution to the amount of damping delivered in the absence of the field. Such a decrease in damping is not desirable as the mount is designed to be fail-safe; i.e., to be operational even when the coils get short-circuited or current cannot be supplied to them. Therefore, the gap of the flow channel was not decreased further—even though this would lead to higher magnetic fields for the same applied electric current. Figure 5(b) illustrates the magnetic flux density distribution inside the MR fluid contained in the flow passage, along a vertical midline, shown as the white dashed line in Fig. 5(a). This distribution indicates a very-close-to-uniform field in the fluid contacting the coil housing and a steep variation in the fluid located near the coil. This result was expected as the coil housing causes the closing of the magnetic flux lines through the MR fluid, unlike the coil itself. The magnetic flux density map inside the mount is shown in Fig. 6(a), while a detailed view of the field distribution through the magnetically active part of the flow channel and on the bottom plate of the squeeze mode is shown in Fig. 6(b).

Based on the simulation results, a decision was also made on the exact configuration of the coils. Accordingly, the coil generating the field for the flow mode (through the flow channel) was made of 400 turns of 25 gauge wire, while the one for the squeeze mode was made of 200 turns using the same wire gauge. The maximum electric current was limited to 2.5 A.

Mathematical modeling: To predict the behavior of the MR mount before its fabrication, a mathematical model was developed based on its physical structure. This model also helps to tune the mount parameters such that its response stiffness and damping characteristics are fit for a specific application. The following assumptions were made in developing this model: The fluid is incompressible, the pressure in each chamber is uniform, and the mount is exposed only to vertical motion. In addition, it was considered that the top of the mount was excited harmonically by a known source (e.g., a shaker) and the bottom of the mount was fixed. Under these assumptions, the equations of motion were derived based on the procedure proposed in Ref. [8].

Accordingly, when the top rubber displaces the flow of the MR fluid through the flow passages it is induced by the pressure difference between the upper and lower chambers. This pressure drop can be expressed by the linear momentum equation:

$$P_1 - P_2 = I_i \dot{Q}_i + R_i Q_i + \Delta P_{MR} \qquad (1)$$

where P_1 is the pressure in the upper chamber, P_2 is the pressure in lower chamber of the mount, I_i is the fluid inertia, R_i is the fluid drag at zero magnetic field, Q_i is the fluid flow rate through the flow passage, and ΔP_{MR} is the pressure drop due to the yield stress of the MR fluid. The fluid pressure in the upper and lower chambers can be calculated from the flow continuity equations [14]:

$$\dot{P}_1 = \frac{A_p}{C_1}\dot{x} - \frac{Q_i}{C_1} \tag{2}$$

$$\dot{P}_2 = \frac{Q_i}{C_2} \tag{3}$$

where C_1 and C_2 are the compliances of the upper and lower chamber, respectively, A_p is the piston area of the top rubber part, $\dot{x}$ is the velocity of the top of the mount.

Assuming $Q_i = A_i\dot{x}_i$, where A_i is the cross sectional area of the flow passage and $\dot{x}_i$ is the fluid average velocity through the flow passage, substituting the integrated forms of equations (2) and (3) into equation (1) yields the following equation of motion for the fluid passing through the flow passage:

$$I_i A_i \ddot{x}_i + R_i A_i \dot{x}_i + A_i\left(\frac{1}{C_1} + \frac{1}{C_2}\right)x_i = \frac{A_P}{C_1}x + \Delta P_{MR} \tag{4}$$

where x is the displacement at the mount top. The pressure difference induced by the MR effect can be expressed as [15]:

$$\Delta P_{MR} = C\frac{L}{h}\tau_y(H)sign(\dot{x}_i) \tag{5}$$

where C is a constant in the range of 2 to 3 depending on the steady-state flow conditions, as suggested in [15]. In this work, it is assumed that C is equal to 2, which corresponds to low-flow conditions. The other parameters appearing in equation (5) are: L is the length inside the flow channel over which the magnetic field is applied, h is the distance between the magnetic poles, which is equal to the gap of the annular duct, b is the width of the channel, $\tau_y(H)$ is the MR fluid yield stress that is magnetic field (H) dependent. The cross section of the flow channel, i.e. orifice, is approximated as a rectangle with the aforementioned dimensions b and h.

The hydraulic related parameters are defined in [16]. Since the flow path is straight, the inertance of the fluid inside the flow passage is $I_i = \frac{\rho L}{A_i}$ where ρ is the density of the MR fluid, L is the length of the flow passage. The fluid resistance within the flow passage is approximated based on the orifice geometry which is rectangular, $R_i = \frac{128\eta L}{\pi D_h^4}$, where η is the MR fluid viscosity, which is shearing rate dependent but assumed to be constant for this study, and $D_h = D_o - D_i = 2h$ is the hydraulic diameter for an annular duct.

The equation of motion pertaining to the squeeze mode is given in [8] as:

$$M\ddot{x} + c_e\dot{x} + k_e x + C_{sq}\dot{x} + F_{sq} + A_p P_1 = F_{in} \tag{6}$$

where F_{in} is the excitation force, c_e and k_e are the rubber damping and stiffness coefficients respectively.

The damping constant associated with the viscous flow is

$$C_{sq} = \frac{3\pi R^3}{2(h_0 + x)^3} \tag{6a}$$

and the damping force due to the fluid squeeze is

$$F_{sq} = \frac{3\pi R^3}{4(h_0 + x)}\tau(H)\text{sign}(\dot{x}) \tag{6b}$$

The variables from the above equations are h_0 – the gap between the parallel plates at the static deflection, and R - the radius of the two plates. After substituting P_1 by equation (2) into (6), the final equation of motion can be written:

$$M\ddot{x} + c_e\dot{x} + \left(k_e + \frac{A_p^2}{C_1}\right)x + C_{sq}\dot{x} + F_{sq} = \frac{A_i A_p}{C_1}x_i + F_{in} \tag{7}$$

Experimental evaluation of the mount

Magnetic force/field investigation: Tests were conducted to examine the magnitude of the magnetic force and field when a current is applied to the squeeze mode electromagnet. These measurements are important because beyond a certain squeeze gap the plates may be attracted to each other inducing an unexpected force in the system. Also, a lack of understanding of this force and its dependence on the squeeze gap may lead to an undesired lock-up state (due to the magnetic attraction) during mount operation. To perform the measurements, the squeeze plate was set parallel to the upper surface of the middle assembly. Then, the gap between the two surfaces was varied and the magnetic force and field were measured for several values of the applied electric current.

Table 1 shows the force measured with a load cell, while Table 2 displays the magnetic field measured with a Hall probe. All the measurements were made in air. The numbers (non-zero forces) corresponding to the Off field are the biased force from the test fixture weight. Analysis of the results listed in Table 1 indicates that the magnetic force developed between the plates is just a fraction of the force applied to the mount during actual testing (i.e. 1000 N in average). Therefore, neglecting this force in the mathematical model should not alter the predicted response of the mount when the squeeze mode is considered. The measurements reported in Table 2 indicate that the magnetic field (measured in air) at an applied current of about 1.0A and above is sufficient to activate the MR fluid.

Table 1 - Magnetic force (in Newtons) induced by the electromagnet in squeeze mode for different gaps and values of the applied electric current.

Gap	Off	0.5A	1.0A	1.5A	2.0A	2.5A	3.0A
2.0mm	15	15.5	17	20	24	29	35
2.5mm	18	18.7	19.8	22	24.5	27.6	31.1
3.0mm	19	19.6	20.3	21.6	23.3	25.5	28
3.5mm	19.5	20	20.4	21.5	22.8	24.4	26.1
4.0mm	20	20.1	20.6	21.3	22.2	23.5	25.1

Table 2 - Magnetic field (in kA/m) measured between the squeeze plates for different gaps and values of the applied electric current.

Gap	Off	0.5A	1.0A	1.5A	2.0A	2.5A	3.0A
2.0mm	3	30	58	86	114	143	170
2.5mm	2	25	48	72	96	119	143
3.0mm	2	21	41	61	81	101	119
3.5mm	1	19	35	53	71	89	105
4.0mm	1	16	31	46	62	78	94

Dynamic stiffness investigation: To evaluate the dynamic stiffness of the mount, experiments were conducted on a BOSE® ElectroForce 3330 system. Pictures (A-6) of the experimental apparatus are included in the Appendix. A known excitation profile was applied to the top of the mount and the transmitted force was measured with a load cell located under the mount. Tests were performed activating the fluid in flow mode only, squeeze mode only, and in both modes simultaneously. The tests were conducted at various levels of magnetic field to determine the effective range of operation of the mount in each mode. The dynamic stiffness was evaluated experimentally for low displacement excitation of 0.2 mm peak-peak and high displacement excitation of 1.0 mm peak-peak. The results for all flow configurations are presented in the following paragraphs.

It may be noted that some of the resulting curves have a zigzag pattern which is due to the controller of the testing machine. During the test, the machine attempts to bring the mount to the desired preload force, i.e. -1000N, before running the cycles. When the control feedback of the machine detects a load undershoot at a test (at a discrete frequency), in the next run (next frequency value), the controller attempts to correct that

and actually overshoots. The under/overshoot happens alternately creating the zigzag pattern. This is a common result for general purpose testing equipment when used for characterization of variable stiffness materials/systems. However, the actual value of the applied preload never over- or under-shoot by more than 3% of the desired preload value, which was considered acceptable. Therefore, the averaged values of the peaks and valleys of the zigzag were used for analysis.

The blue solid curve plotted in Figure 7 displays the dynamic stiffness of the mount when no current is applied. Upon activation of the flow mode, an increase of the electric current translates in an increase in the applied magnetic field that determines an increase in stiffness at lower frequencies and decrease in stiffness at higher frequencies. In other words, a higher magnetic field flattens the dynamic stiffness profile, increasing the stiffness at low frequencies and decreasing it at high frequencies. The dynamic stiffness depends strongly on the damping induced by the fluid flowing through the channel. The stiffness decreases at high frequencies when the applied field increases; this is due to the reduced fluid volume flowing through the passage at high frequency. The high magnetic field causes a similar change in the response characteristic of the mount as a narrower flow passage, i.e., it makes it harder for the flow to happen. Therefore, at high frequency, the amount of flow through the passage is small which leads to small damping, i.e. decreased dynamic stiffness. For the 0.3A case, the magnetic field is large enough to block the fluid flow through the channels making the mount exhibit a dynamic stiffness profile similar to that of a simple rubber mount, i.e. an almost constant dynamic stiffness. At this end, the effect of the MR fluid on the damping/stiffness is saturated, and the "flat" curve corresponding to 0.3A is called a "saturation line" for later reference.

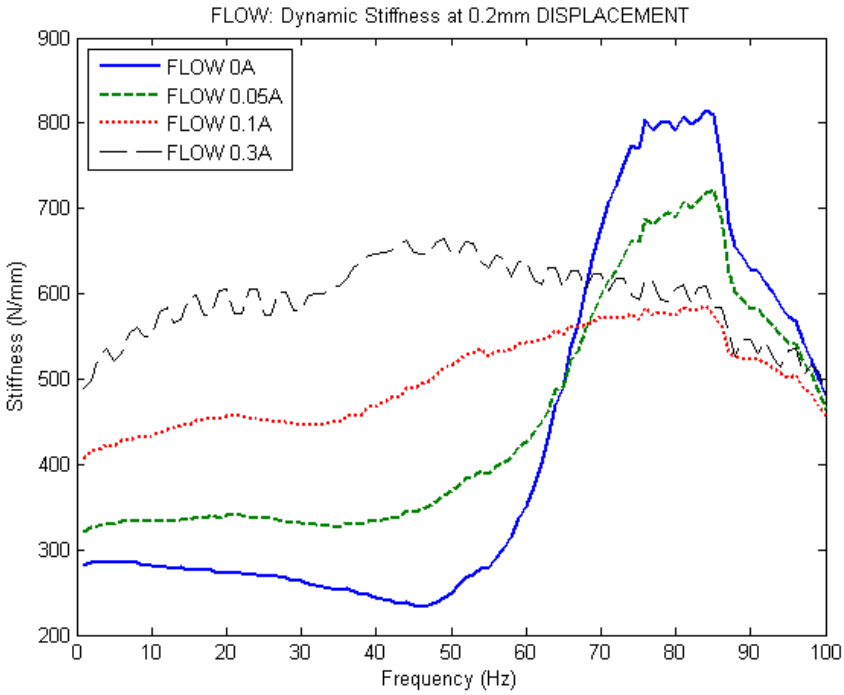

Figure 7 Flow mode only, displacement excitation of 0.2 mm.

The dynamic stiffness expresses how much force is transmitted through the mount. The significant decrease in dynamic stiffness at the peak, from 800N/mm to about 550N/mm, upon the application of the electric current indicates the capability of the MR mount in maintaining low transmitted force.

The dynamic stiffness measured at amplitudes of excitation of 1.0 mm (see Figure 8) displays a similar pattern with the 0.2 mm amplitude of excitation shown in Figure 7. The dynamic stiffness curves also flatten at high applied current levels. As all the dynamic stiffness lines cross through almost the same point (see Figure 8), this can be considered as the dividing point between low and high frequency ranges.

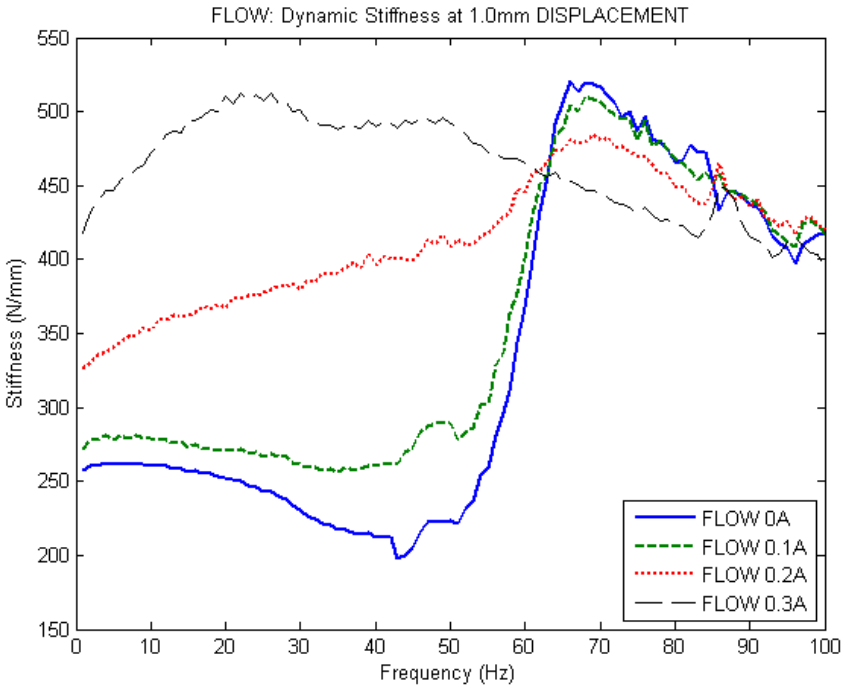

Figure 8 Flow mode only, displacement excitation of 1.0 mm.

A direct comparison between 0.2 mm and 1.0 mm excitations for flow mode only is illustrated in Figure 9. It can be seen that at low excitations, the mount exhibits higher dynamic stiffness than at high excitations, in both field on and field off conditions. This effect is due to the characteristics of the rubber and the amount of fluid (fluid inertia) passing through the flow channel. The saturation line in the case of 1.0 mm excitation has a smaller amplitude than in the case of 0.2 mm excitation. However, the saturation line for 1.0 mm excitation exhibits a higher percentage of change in dynamic stiffness than the one for 0.2 mm. Hence, the flow mode is more effective in the high excitation case.

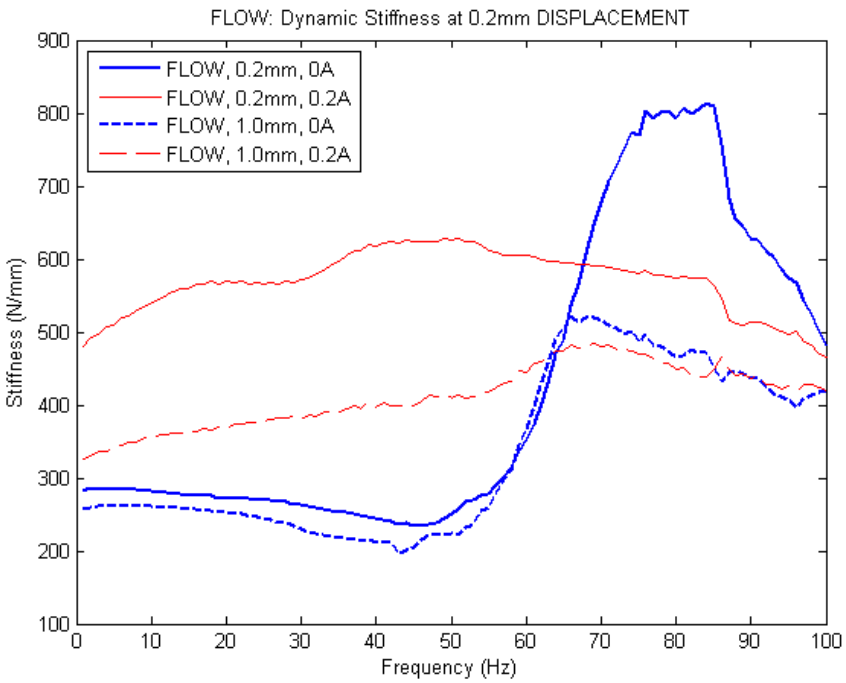

Figure 9 Flow mode only, displacement excitation 0.2 mm vs. 1.0 mm.

Figures 10, 11 and 12 display the results of the experiments performed with only the squeeze mode activated. These results indicate a similar trend, i.e., when the applied current increases, the entire dynamic stiffness profile is shifted upward.

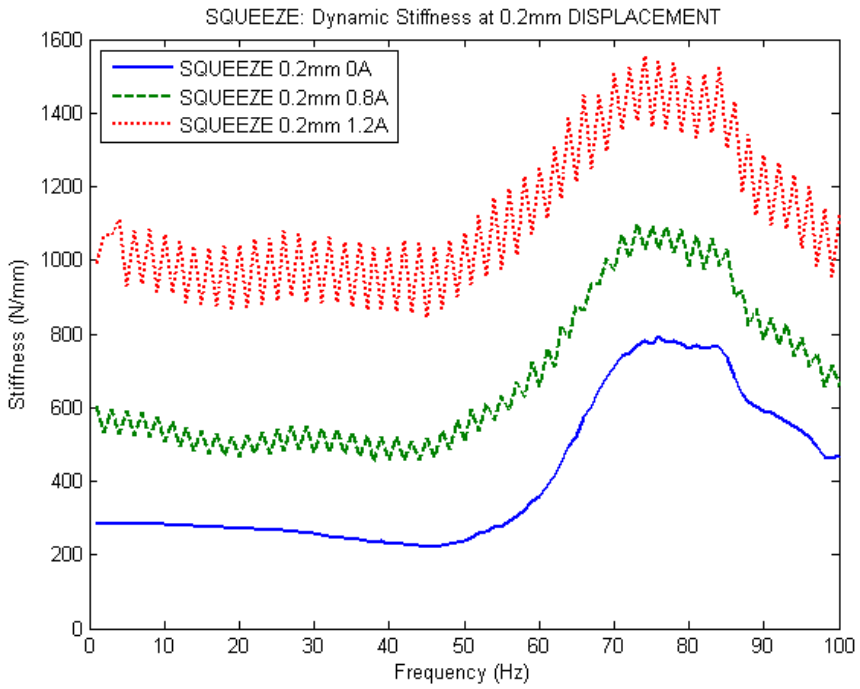

Figure 10 Squeeze mode only, displacement excitation of 0.2 mm.

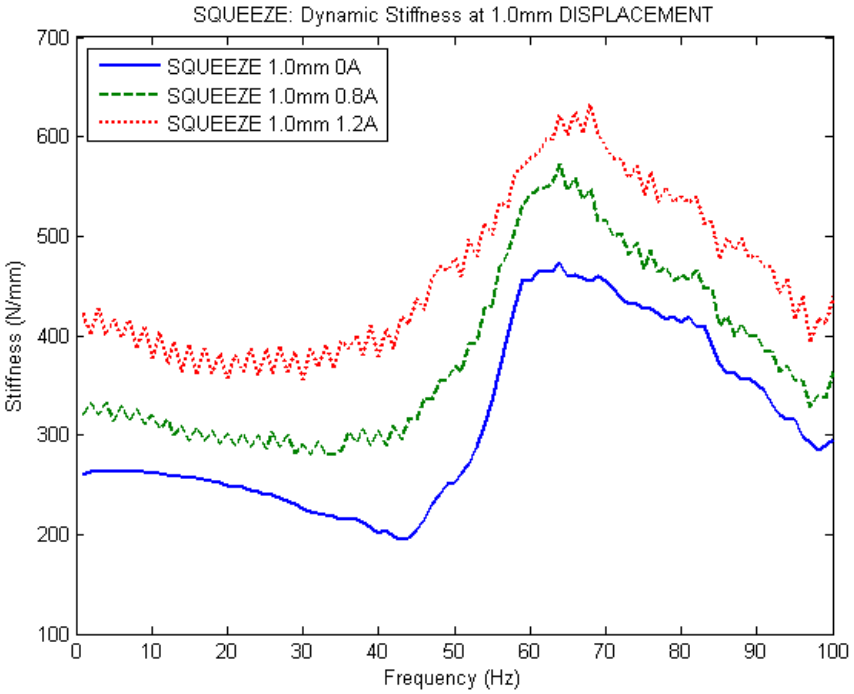

Figure 11 Squeeze mode only, displacement excitation of 1.0 mm.

Figures 12 and 13 show that the upward shift is fairly uniform within the full range of frequency. This trend can be explained from observing the spring-like structure of the chains formed in a vertical direction as the squeeze mode is activated. Therefore, when the field is on, the squeeze mode acts similarly to an elastic spring. Higher magnetic field yields higher spring stiffness. This high stiffness is desirable in case of shock loads to quickly mitigate their effect.

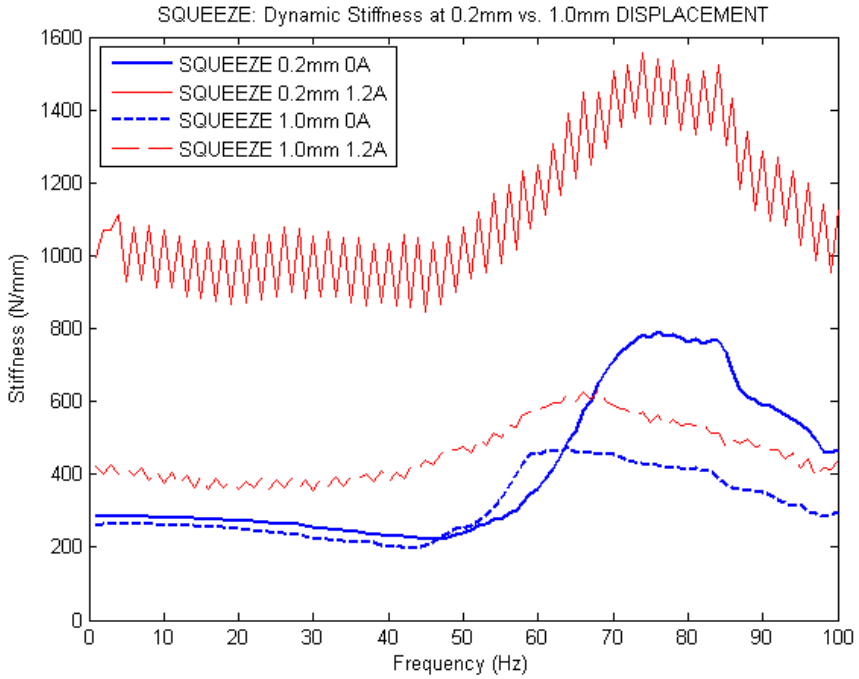

Figure 12 Squeeze mode only, displacement excitation of 0.2 mm vs. 1.0 mm.

Figure 12 shows the effect of the fluid activation on the response of the mount at low and high amplitudes of excitation. Dynamic stiffness for the 0.2 mm excitation increases about four times as the current is applied. On the other hand, the dynamic stiffness for the 1.0 mm excitation only doubles with the applied current. These results show that the squeeze mode works more effectively in changing the dynamic stiffness at a low excitation level.

The results of the combined mode are displayed in Figures 13 and 14. They both indicate an identical pattern which is described as follows: when only the flow mode is turned on (red dotted line), the dynamic stiffness flattens to a certain level between the notch and the peak amplitudes; when only the squeeze mode is turned on, the entire dynamic stiffness is shifted upward; finally, when both modes are turned on, the flat dynamic stiffness is shifted upward for an approximate amount of the squeeze mode effect. This means each mode has a separate effect on the mount, which is not affected by the other.

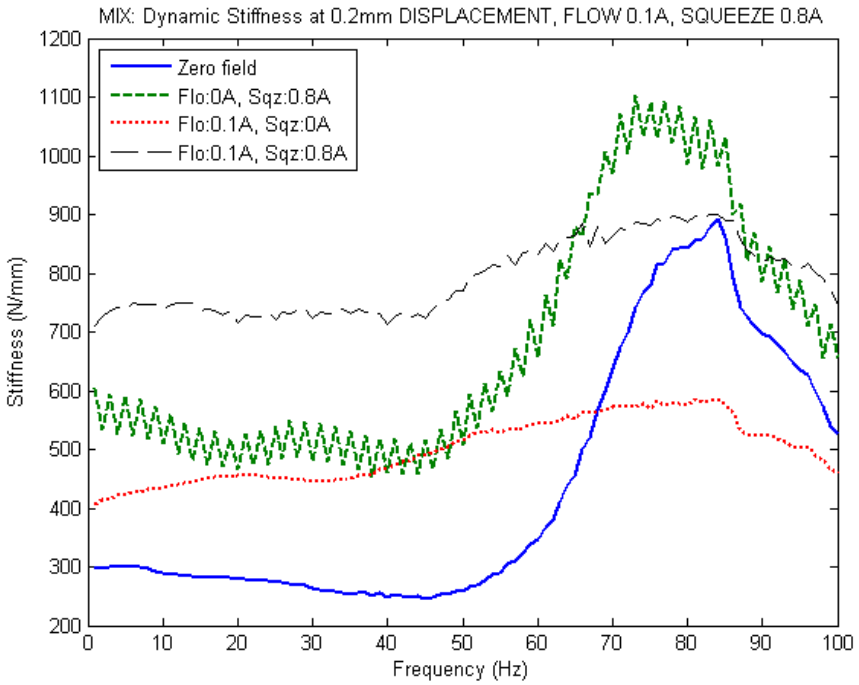

Figure 13 Combined mode, displacement excitation of 0.2 mm.

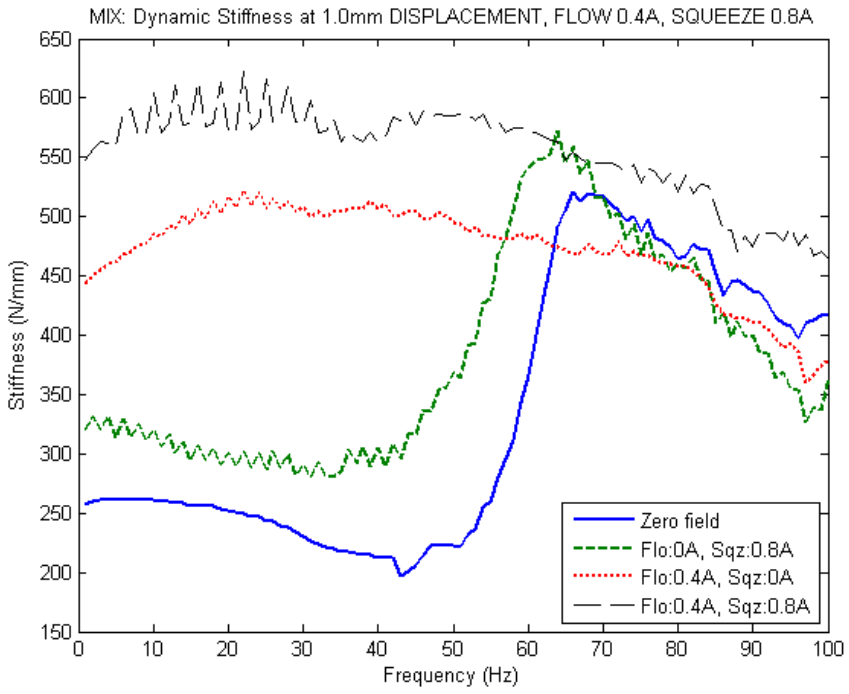

Figure 14 Combined mode, displacement excitation of 1.0 mm.

The amplitudes of the dynamic stiffness express the independent effect, i.e. non-interference, of each mode. For example, in Figure 14, the black dashed curve is a close-to-identical copy of the red dotted curve (flow mode effect) but with about 300N/mm

higher in amplitude (squeeze mode effect seen in the amplitude difference between green and blue curves). In other words, the combined mode is the superposition of the individual modes, which leads to the benefits summarized in Figure 15.

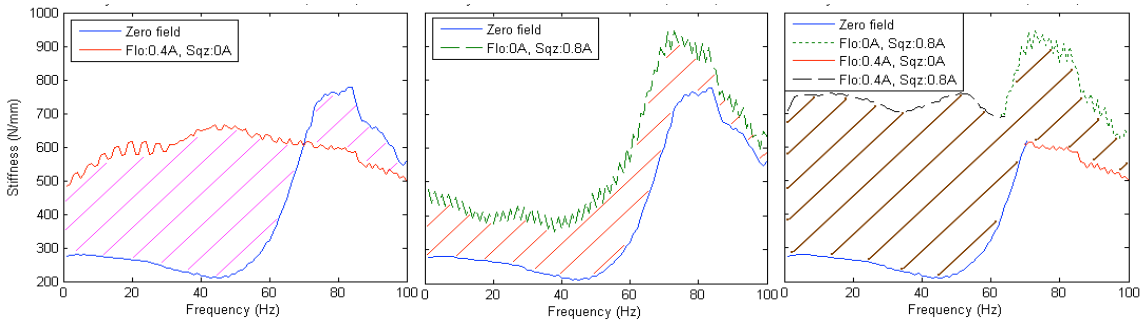

Figure 15 - Comparison in performance of individual modes and combined mode at 0.4mm displacement.

Figure 15 highlights the improvement of the combined mode to the overall response of the mount compared to the response for individual modes. Graph (a) expresses the region that the dynamic stiffness of the mount can be if using only flow mode. The stiffness of the mount can be anywhere within the pink shaded region. Graph (b) displays the capability of the mount if only squeeze mode is employed. The mount stiffness can achieve any level covered by the orange shade. Graph (c) illustrates the capability of the mount if both flow and squeeze modes can be utilized simultaneously. The brown shaded area is approximately equal to the combination of the other two regions. This feature of the mixed-mode MR mount enables the use of this device in a wide range of applications.

Figure 16 illustrates the ability of the mathematical model in predicting the response of the mount in flow mode only, squeeze mode only and for a combination of both modes. From Fig. 16(a), it can be seen that the theoretical model is able to predict precisely the behavior of the mount working only in flow mode when the applied current is small. At a higher applied current, i.e. higher magnetic field, the prediction is good within the middle range of frequency. A small discrepancy happens at the beginning. This inaccuracy does not happen to the squeeze mode as shown in Fig. 16(b). The analytical simulated results approximate closely the experimental ones. These results are also close when both modes are activated, as displayed in Fig. 16(c). The error between the simulated curve and the experimental curve is minimal in the whole range of frequencies.

It should be noticed that the predicted results only approximate the experimental ones from zero until about 85Hz. This phenomenon can be seen in all figures. This is due to the fact that the mount is not absolutely degassed. When a small amount of air is trapped in the mount and mixes with the fluid, the stiffness of the mount declines sharply at the high frequency range, i.e., after the peak. This study has not been able to explain the mount response due to the trapped air. Therefore, the mathematical model can only predict the behavior of the mount up to 85Hz. Despite the mismatch between simulated and experimental data above 85Hz, the analytical model is capable of forecasting the

response of the mount within the most common range of the mount's operating frequency. The model is therefore useful for the control of the mount.

Control of the MR mount

Without a controller, the MR mount developed in the research works only as effective as a passive isolation. The control system is designed to adjust the behavior of the system in order to function effectively in various working conditions. In other words the control logic adjusts damping and stiffness of the system so that the system can minimize the noise and vibration transmissibility.

A simple Skyhook controller has only one reference value. That design can cause the non-smooth transition between states of the MR damper. Alternatively, a modified Skyhook controller, which utilizes multiple reference values, was designed. In ON states, the damping force amplitude depends on the magnitude of the reference values. The bigger the reference value, the greater damping force is applied. With these multiple ON states, the difference between damping forces is smaller, so the transition is smoother.

The following equations show structures of the simple Skyhook and modified Skyhook algorithm:

Simple Skyhook:
$$\zeta_{MR} = \begin{cases} 0 & If \quad \left|\dot{x}_P\right| < \dot{x}_{ref} \\ \zeta_0 = .02 & If \quad \left|\dot{x}_P\right| \geq \dot{x}_{ref} \end{cases}$$

Modified Skyhook:
$$\zeta_{MR} = \begin{cases} 0 & If \quad \left|\dot{x}_P\right| < \dot{x}_{ref1} \\ \zeta_1 & \\ \zeta_2 & If \quad \dot{x}_{ref1} \leq \left|\dot{x}_P\right| < \dot{x}_{ref2} \\ ..... & If \quad \dot{x}_{ref2} \leq \left|\dot{x}_P\right| < \dot{x}_{ref3} \\ \zeta_{\mathbf{n}} & ..... \\ & If \quad \left|\dot{x}_P\right| \geq \dot{x}_{ref\mathbf{n}} \end{cases}$$

ζ is the damping ratio of the mount. The damping ratio is increasing $(0 < \zeta_1 < \zeta_2 < ... < \zeta_{\mathbf{n}})$ when the reference value of velocity is increasing $(0 < \dot{x}_{ref1} < \dot{x}_{ref2} < ... < \dot{x}_{ref\mathbf{n}})$.

These skyhook control methods are effective because they can deliver variable damping effects to the mounting system. The mount can have high damping within a low frequency range when the MR element is ON, and low damping within the high frequency range when the MR element is OFF. The skyhook algorithm simultaneously achieves simplicity and effectiveness.

The three figures 17-19 illustrate the comparison of those methods. These figures show the advantages that the modified skyhook controller has over the simple one. First, the damping force provided from the MR element using the modified skyhook algorithm is always less than the one using the simple skyhook algorithm. Thus, that modification helps to save energy. Second, the damping force provided by ON states of the MR component is proportional to the velocity reference value in the modified skyhook structure, i.e. the bigger velocity of the hybrid vehicle results in the larger damping force provided from the MR element. Figures 17 to 19 show the difference in smoothness of the curves indicating the smoother damping effects to the system when using the modified skyhook controller.

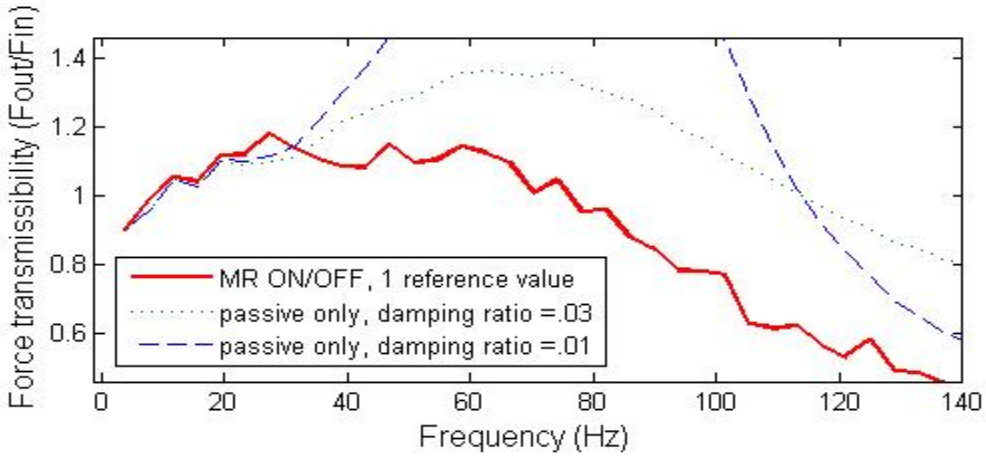

Figure 17 Force transmissibility curve of MR controlled ON/OFF with only one velocity reference value is oscillatory.

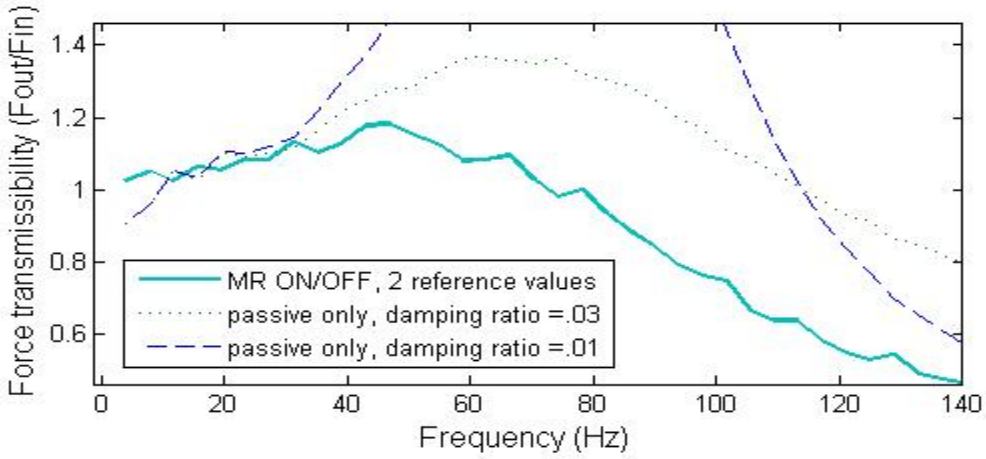

Figure 18 Force transmissibility curve of MR controlled ON/OFF with two velocity reference values shows a smoother trace.

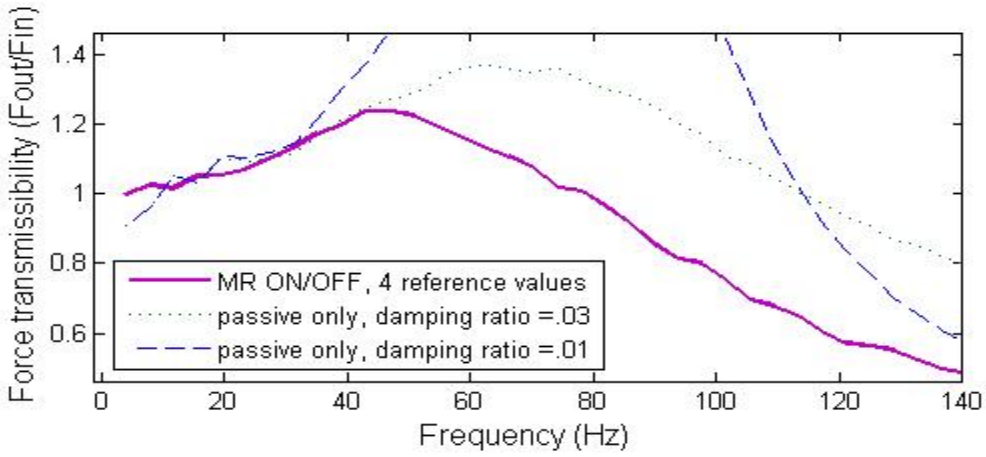

Figure 19 Force transmissibility curve of MR controlled ON/OFF with four velocity reference values has a smooth path.

Experimental evaluation of the controller: Dynamic stiffness is one of the main characteristics of the system. The main function of the controller is to regulate the magnetic field in order for the mount to achieve and deliver the desired level of dynamic stiffness. From the experimental results, the dynamic stiffness calculation is shown in the following equations.

$$\begin{aligned} &\textit{Displacement Excitation} && x(t) \rightarrow X(\omega) = FFT(x) \\ &\textit{Transmitted Force} && f(t) \rightarrow F(\omega) = FFT(f) \\ &\textit{Dynamic Stiffness} && K_{dyn}(\omega) = \frac{F(\omega)}{X(\omega)} = A + iB \end{aligned}$$

$$Amplitude = \left|K_{dyn}\right| = \sqrt{A^2 + B^2}; \qquad Phase = \tan^{-1}\left(\frac{B}{A}\right)$$

The force and displacement transmissibilities are two other indicators for the performance of the mount as defined for experimental evaluation with the following equations.

$$\begin{aligned} &\textit{Force Excitation} && f_{in}(t) \rightarrow F_{in}(\omega) = FFT(f_{in}) \\ &\textit{Transmitted Force} && f_{out}(t) \rightarrow F_{out}(\omega) = FFT(f_{out}) \\ &\textit{Transmissibility} && TR(\omega) = \frac{F_{out}(\omega)}{F_{in}(\omega)} = C + iD \end{aligned}$$

$$Amplitude = \left|TR\right| = \sqrt{C^2 + D^2}; \quad Phase = \tan^{-1}\left(\frac{D}{C}\right)$$

The mount provides a high dynamic stiffness at lower frequencies and a lower dynamic stiffness at higher frequencies caused by the switching. In other words, a certain dynamic stiffness profile corresponds to a certain transmissibility profile. Therefore, dynamic stiffness is the major indicator of the transmissibility. In the experiments, this figure of merit has been used as a measurement for vibration transmissibility. The control law adopted here is a proportional control. Based on the envelope values for a certain frequency, a linear increase of the dynamic stiffness is assumed due to the increase of the current. For instance, at 20Hz the dynamic stiffness without any field is about 255 N/mm as a low base line, while the dynamic stiffness with the current at 0.4A for the flow mode is about 380 N/mm as a high base line. Therefore, the difference of dynamic stiffness (380 N/mm-255/mm=125 N/mm) is caused by 0.4 A. Then a unit increase of dynamic stiffness can be caused by 0.4/125 A. For the desired dynamic stiffness, the necessary current can be calculated by the difference between its value and the low base line times the current causing the unit increases of dynamic stiffness. If 350N/mm dynamic stiffness is desired to be achieved at 20Hz, the desired current to realize that will be (350-255)*0.4/125=0.304A.

As the simulations for the control of the MR fluid mount in the single degree of freedom and two degrees of freedom have been conducted, one question is left: Can the desired dynamic stiffness (which corresponds to the lowest transmissibility) be achieved by the prototype mount and testing machine? If the desired dynamic stiffness at certain frequencies can be obtained by the control of the current, it is equivalent to achieve the desired lowest transmissibility at that frequency. This could lead to achieving the desired lowest transmissibility at the entire working frequency range. The experiments have been

conducted at frequencies under 30 Hz. The flow mode is chosen to achieve the desired dynamic stiffness (DS). The close match between desired and achieved DS can be observed in Figure 20.

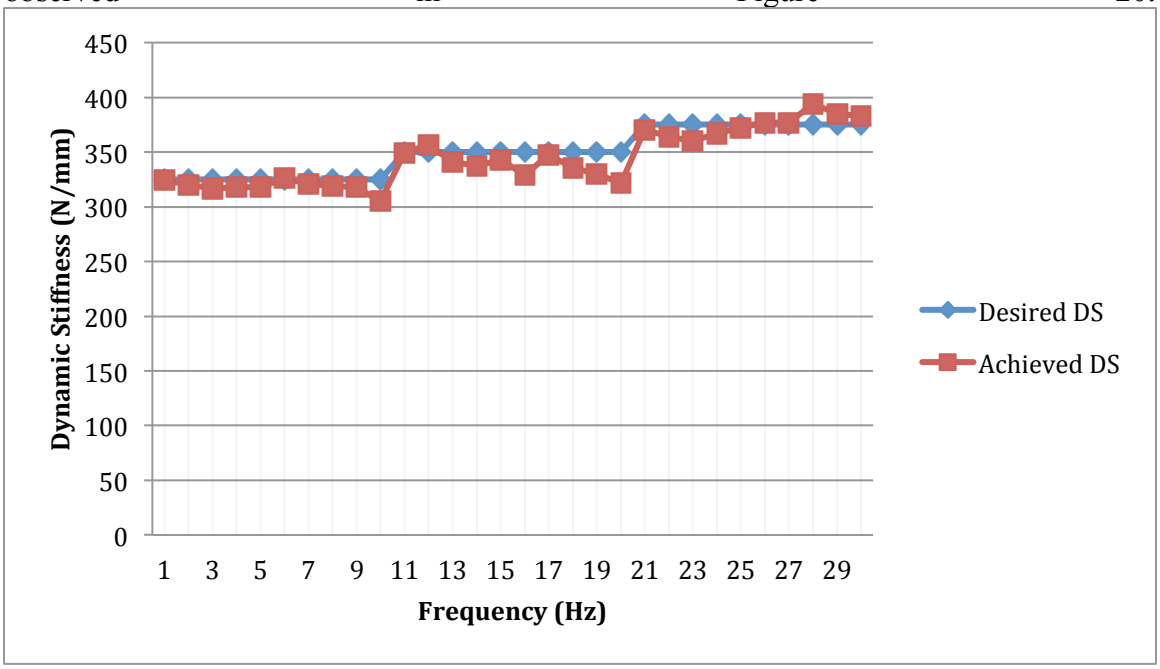

Figure 20 Comparison between desired dynamic stiffness (DS) and achieved stiffness

The largest error that occurred in the tests was 8.12%, and the smallest error was 0.14%. The average error was 2.69%. The error is an indicator of the good tracking ability for the desired dynamic stiffness.

As it shows, for each frequency, the desired dynamic stiffness is set. Take 24 Hz for an example: the target is 375 N/mm, the experimental result is about 367 N/mm. The dynamic stiffness at a certain frequency can be closely achieved. This makes possible the desired dynamic stiffness profile over the whole working frequency.

The sine wave is tested for 10Hz to verify that the variable dynamic stiffness can be achieved for a certain frequency. The squeeze mode is chosen for this test. The sine wave is

$$\text{sine wave} = 25 * \sin(\pi * t) + 315$$

The desired dynamic stiffness profile fluctuates around 315 N/mm and the fluctuation range is 25 N/mm as shown in the layout of ControlDesk software, see the red line in Figure 21.

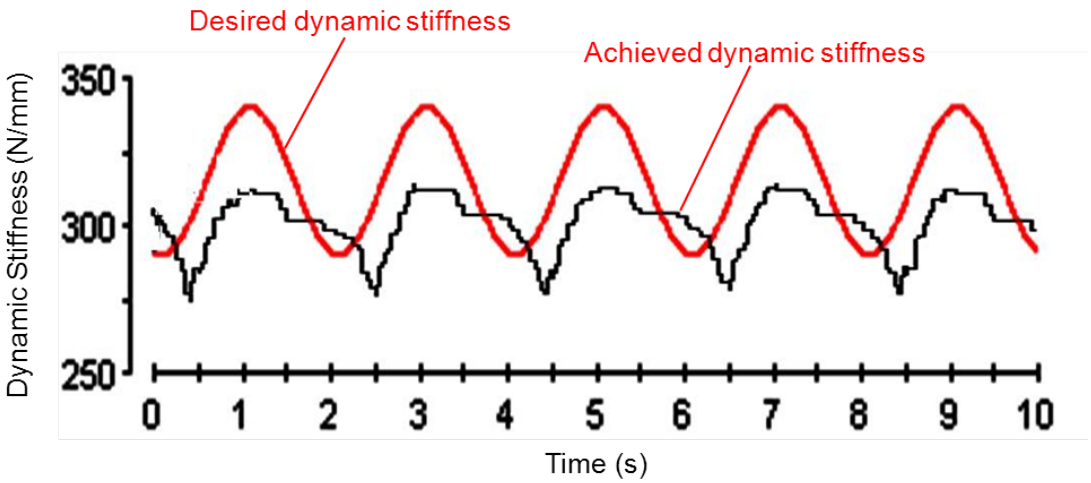

Figure 21: Desired dynamic stiffness profile

The dynamic stiffness achieved is shown in black. The range of the achieved dynamic stiffness is from about 275 to 315. The mean value is 295. The error can be roughly calculated by the following:

$$(340 - 315)/340 * 100\% = 7.35\%$$
$$(315 - 295)/315 * 100\% = 6.35\%$$
$$(290 - 275)/290 * 100\% = 5.17\%$$

The largest error is about 7.35%, the smallest error is about 5.17%, and the average error is about 6.35%. These results are acceptable for the experiment.

This part of the experiment proves that the variable dynamic stiffness at a certain frequency can be approximately achieved. It can be inferred that the variable dynamic stiffness can be achieved over a range of frequencies. Consider the two degrees of freedom model: the lowest displacement transmissibility and lowest force transmissibility correspond to different dynamic stiffness profiles. The experiment shows that switching between two dynamic stiffness profiles can be obtained.

In summary, the experiments complete the verification of the model and control of the mixed mode MR fluid mount. It can be concluded by simulations and by experiments that the proposed MR fluid mount is able to provide a certain range of dynamic stiffness over a large range of frequencies and also the desired dynamic stiffness could be achieved in reality.

Conclusions: In summary, the results of this study are promising and demonstrate the feasibility of the concept consisting in the modification of the mount stiffness by means of activation of an MR fluid.

When the mount works only in flow mode, its dynamic stiffness profile flattens to an average level between the peak and the notch. At the saturation level, when the magnetic

field is strong enough to block the fluid flow, the mount behaves similarly to a stiff rubber block.

When only the squeeze mode is activated, the mount is stiffened uniformly in the entire range of frequencies. The dynamic stiffness rises proportionally to the amplitude of the magnetic field. Application of a high electric current leads to a magnetic field strong enough to cause an increase in the mount stiffness of several orders of magnitude. To that end, the effect of the hydraulic flow diminishes and the mount response is due only to the squeeze mode and the top rubber effects.

The combined mode can be observed as the superposition of the two individual modes. Each mode does not interfere or restrain the effect of the other. The individual modes can be manipulated in an efficient way to maximize the potential of the mount.
The mixed-mode mount expands significantly the amplitude margins (between the notch and peak) of a passive hydraulic mount. The dynamic stiffness envelope is very large allowing the users to have a desired stiffness at any frequency. In addition, the ability to set the dynamic stiffness for any excitation amplitude optimizes the vibration isolation process.

This mixed-mode MR mount outperforms the other single-mode and combined-mode MR mounts due to the independence of the modes. The mixed mode can raise the dynamic stiffness amplitude multiple times in the low frequency range while the flow mode alone can drop the dynamic stiffness in half at the high frequency range. The mount can be stiff for shock mitigation and soft for harmonic vibration isolation. This feature also provides the flexibility to design the optimal control schemes for the mount with the least energy consumption. The combined modes extend the capability of the mount to meet the requirements of various applications. Furthermore, as no shear mode effect was detected, this highlights the success of the mount design which aimed for only flow and squeeze operating modes. In the project, a controller also was designed and numerically evaluated for the MR mount. This controller was evaluated on the MR mount in closed-loop mode. To this end, the controller designed in this work was implemented in a micro-controller and applied to the MR mount that was previously fabricated and evaluated.

Acknowledgment
This work was supported by a grant from the US Department of Transportation through The University of Toledo University Transportation Center. The author would like to acknowledge this financial support.

Reference

[1] Yu, Y., Naganathan, N. G., and Dukkipati, R. V., 2001, “A Literature Review of Automotive Vehicle Engine Mounting Systems,” Mech. Mach. Theory,
36(1), pp. 123–142.
[2] Singh, R., Kim, G., and Ravindra, P. V., 1992, “Linear Analysis of Automotive

Hydro-Mechanical Mount With Emphasis on Decoupler Characteristics," J. Sound Vib., 158(2), pp. 219–243.
[3] Carlson, D., Catanzarite, D., and Clair, K. S., 1995, "Commercial Magneto Rheological Fluid Devices," Proceedings of the 5th International Conference on ER Fluids, Magneto-Rheological Fluids and Related Phenomenon, Sheffield, United Kingdom, July 10–14.
[4] Ahn, Y., Ahmadian, M., and Morishita, S., 1999, "On the Design and Development of a Magneto-Rheological Mount," Veh. Syst. Dyn., 32, pp. 199–216.
[5] Ahmadian, M., and Ahn, Y., 1999, "Performance Analysis of Magneto-Rheological Mounts," J. Intell. Mater. Syst. Struct., 10, pp. 248–256.
[6] Stelzer, G. J., Schulz, M. J., Kim, J., and Allemang, R. J., 2003, "A Magnetorheological Semi-Active Isolator to Reduce Noise and Vibration Transmissibility in Automobiles," J. Intell. Mater. Syst. Struct., 14, pp. 743–765.
[7] Ahn, Y., Yang, B., Ahmadian, M., and Morishita, S., 2005, "A Small-Sized Variable-Damping Mount Using Magnetorheological Fluid," J. Intell. Mater. Syst. Struct., 16(2), pp. 127–133.
[8] Hong, S. R., Choi, S. B., Jung, W. J., and Jeong, W. B., 2002, "Vibration Isolation of Structural Systems Using Squeeze Mode ER Mounts," J. Intell. Mater. Syst. Struct., 13, pp. 421–424.
[9] Hong, S. R., Choi, S. B., and Lee, D. Y., 2006, "Comparison of Vibration Control Performance Between Flow and Squeeze Mode ER Mounts: Experimental Work," J. Sound Vib., 291, pp. 740–748.
[10] Barber, D. E., and Carlson, D. J., 2008, "Performance Characteristics of Prototype MR Engine Mounts Containing LORD Glycol MR Fluids," ERMR 2008 Conference, Dresden, Germany.
[11] Arzanpour, S., and Golnaraghi, M. F., 2008, "A Novel Semi-Active Magnetorheological Bushing Design for Variable Displacement Engines," J. Intell. Mater. Syst.Struct., 19, pp. 989–1003.
[12] Arzanpour, S., and Golnaraghi, M. F., 2008, "Development of a Bushing With an Active Compliance Chamber for Variable Displacement Engines," Veh. Syst. Dyn., 46(10), pp. 867–887.
[13] Arzanpour, S., and Golnaraghi, M. F., 2010, "Development of an Active Compliance Chamber to Enhance the Performance of Hydraulic Bushings," ASME J. Vibr. Acoust., 132, pp. 110–118.
[14] Woods, R. I., and Lawrence, K. L., 1997, Modeling and Simulation of Dynamic Systems, Prentice Hall, London.
[15] Srinivasan, A. V., and McFarland, M. D., 2001, Smart Structures: Analysis and Design, Cambridge University Press, New York.
[16] Adiguna, H., Tiwari, M., Singh, R., Tseng, H. E., and Hrovat, D., 2003, "Transient Response of a Hydraulic Engine Mount," J. Sound Vib., 268, pp. 217–248.

Appendix A
Fabricated mount and experimental apparatus

Fig. A-1: Inner coil assembly.

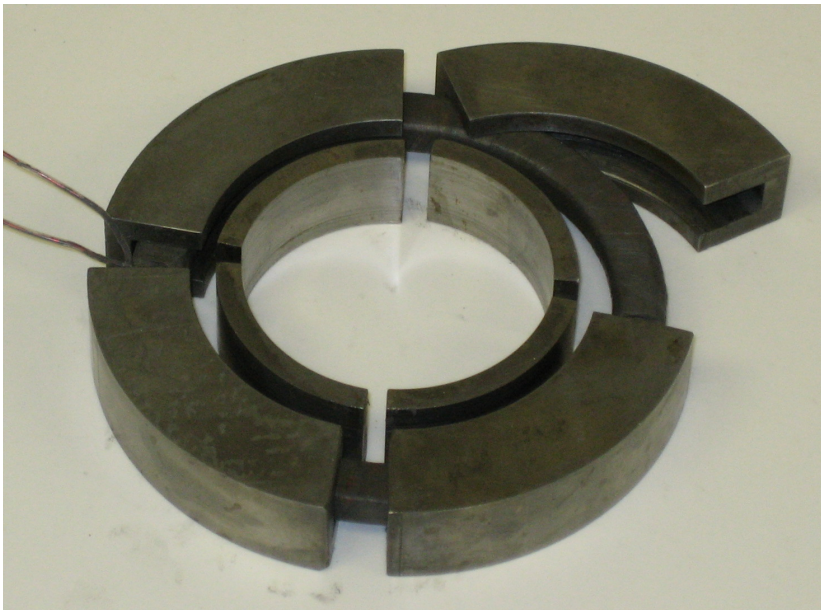

Fig. A-2: Outer coil assembly

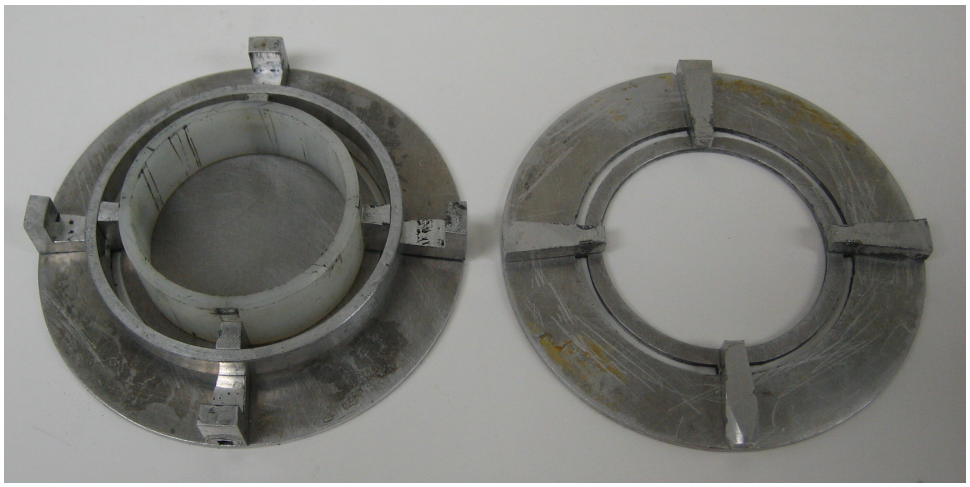

Fig. A-3: Lower (left) and upper (right) plates.

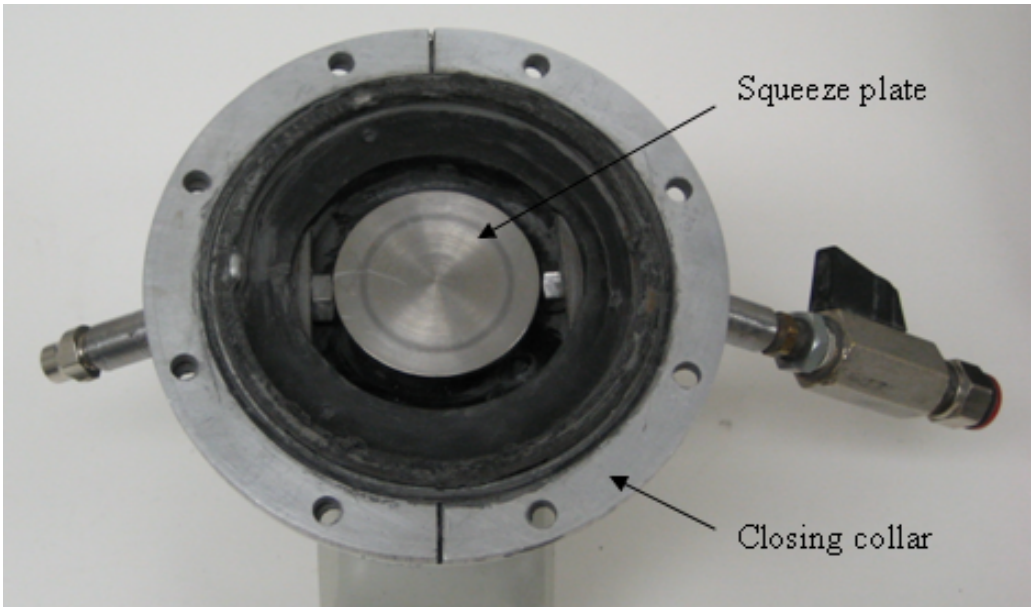

Fig. A-4: Bottom view of the upper part.

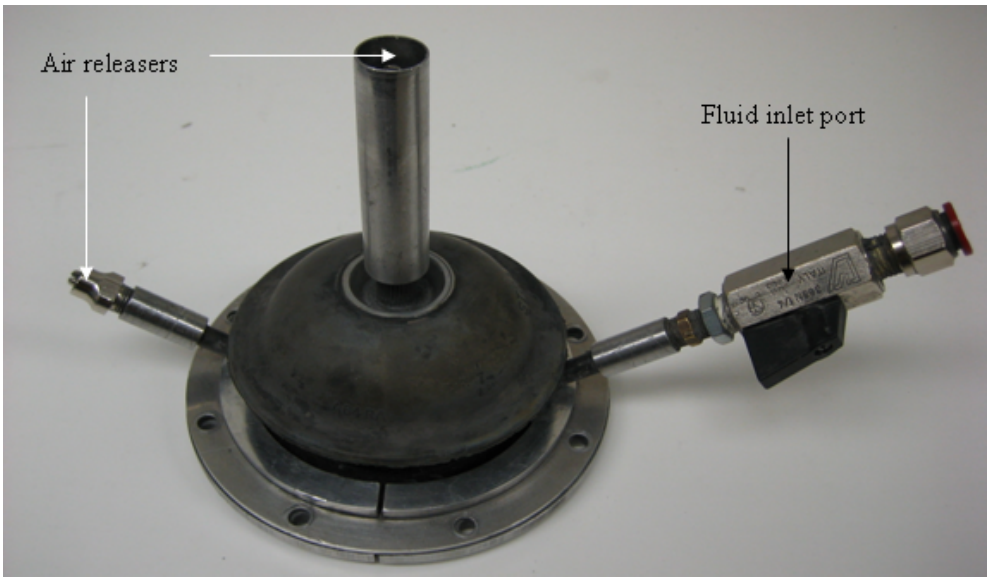

Fig. A-5: Bird's eye view of the upper part.

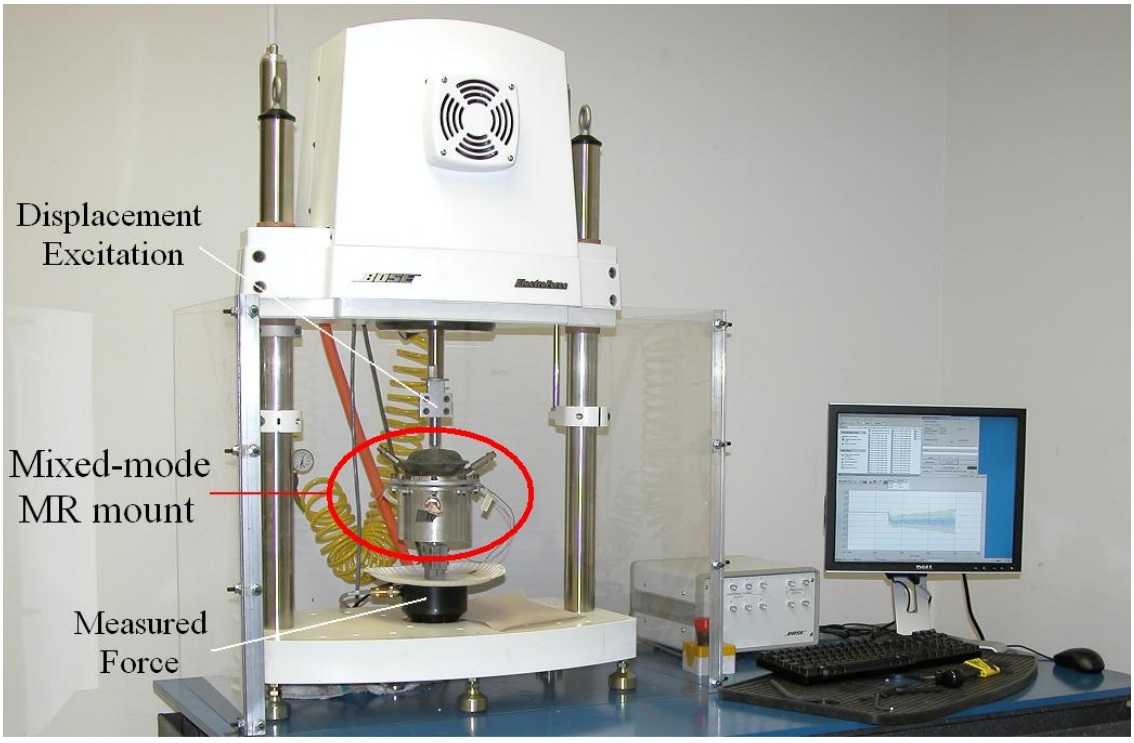

Fig. A-6: Experimental setup – Bose Machine on the left (white color), PCI box and analytical program on the right.